Article

Neuron

GLUT4 Mobilization Supports Energetic Demands of Active Synapses

Highlights

- The glucose transporter GLUT4 is present at nerve terminals
- Neuronal activity recruits GLUT4 to presynaptic plasma membrane
- GLUT4 is required for synaptic function during sustained activity
- AMP kinase drives GLUT4 mobilization during activity

Authors

Ghazaleh Ashrafi, Zhuhao Wu, Ryan J. Farrell, Timothy A. Ryan

Correspondence

taryan@med.cornell.edu

In Brief

Ashrafi et al. identify the glucose transporter GLUT4 as a metabolic modulatory system that upregulates glycolysis in firing neurons to meet activity-driven ATP demand at nerve terminals. This GLUT4 regulatory module is essential for sustained synaptic transmission.

Ashrafi et al., 2017, Neuron *93*, 606–615
February 8, 2017
http://dx.doi.org/10.1016/j.neuron.2016.12.020

CellPress

CellPress

Neuron
Article

GLUT4 Mobilization Supports Energetic Demands of Active Synapses

Ghazaleh Ashrafi,[1] Zhuhao Wu,[2] Ryan J. Farrell,[1,2] and Timothy A. Ryan[1,3,*]
[1]Department of Biochemistry, Weill Cornell Medicine, New York, NY 10021, USA
[2]Laboratory of Brain Development and Repair, The Rockefeller University, New York, NY 10065, USA
[3]Lead Contact
*Correspondence: taryan@med.cornell.edu
http://dx.doi.org/10.1016/j.neuron.2016.12.020

SUMMARY

The brain is highly sensitive to proper fuel availability as evidenced by the rapid decline in neuronal function during ischemic attacks and acute severe hypoglycemia. We previously showed that sustained presynaptic function requires activity-driven glycolysis. Here, we provide strong evidence that during action potential (AP) firing, nerve terminals rely on the glucose transporter GLUT4 as a glycolytic regulatory system to meet the activity-driven increase in energy demands. Activity at synapses triggers insertion of GLUT4 into the axonal plasma membrane driven by activation of the metabolic sensor AMP kinase. Furthermore, we show that genetic ablation of GLUT4 leads to an arrest of synaptic vesicle recycling during sustained AP firing, similar to what is observed during acute glucose deprivation. The reliance on this biochemical regulatory system for "exercising" synapses is reminiscent of that occurring in exercising muscle to sustain cellular function and identifies nerve terminals as critical sites of proper metabolic control.

INTRODUCTION

Regulatory metabolic pathways ensure fuel availability for the proper function of various body tissues. These pathways are particularly important for organs that undergo rapid changes in metabolic demand such as striated muscle and brain. The brain, while only representing ~2.5% of body mass, accounts for ~20% of energy expenditure, and like the heart, it is never in a fully "resting" state, undergoing rapid local changes in activity. In order to maintain function, such changes in activity must be accompanied by a corresponding upregulation of fuel availability. Not surprisingly, cognitive function is closely linked to the metabolic state of the brain: acute interruptions in fuel supply, as experienced by neurons during ischemic events or bouts of hyperglycemia, generally lead to profound and immediate suppression of neuronal function. These examples underscore the general vulnerability of brain function to the maintenance of proper metabolic support and illustrate the need to dissect how neuronal activity regulates fuel usage and availability. The biochemical mechanisms responsible for regulating fuel availability in neurons, however, are poorly understood and have likely been obscured by the fact that chronic genetic ablation of fuel delivery pathways often result in maladaptive compensations (Abel et al., 1999). We recently showed that electrical activity at nerve terminals drives new glycolysis that is required to sustain synaptic vesicle (SV) recycling (Rangaraju et al., 2014). Glucose is the main energy source of the brain, and nerve terminals are enriched in the machinery for glycolysis, as five of the ten essential glycolytic enzymes co-purify with SVs (Ikemoto et al., 2003; Knull and Fillmore, 1985). Moreover, recent in vivo studies have shown that a local glycolytic "metabolon" forms in nerve terminals during energy deprivation and neuronal activity (Jang et al., 2016). However, the cellular and molecular mechanism by which activity drives nerve terminal glycolysis is unknown. It has long been known that exercise increases glucose uptake in muscle compared to at rest (Chauveau and Kaufmann, 1887) by contraction-driven insertion of the glucose transporter GLUT4 into the plasma membrane (Douen et al., 1990; Lauritzen et al., 2010; Roy and Marette, 1996) through a mechanism that is distinct from insulin-driven regulation of GLUT4 in this tissue. We therefore hypothesized that neuronal activity may similarly recruit a glucose transporter to presynaptic surface. While GLUT3 is the canonical glucose transporter in neurons (Gerhart et al., 1992), the expression of GLUT4 in several brain regions, including the cortex, hippocampus, cerebellum, and olfactory bulb, has been reported (Kobayashi et al., 1996; Vannucci et al., 1998). The functional significance of GLUT4 in the nervous system, however, has remained unknown. Here, we show that GLUT4 is present at hippocampal nerve terminals, and we uncover a novel paradigm whereby GLUT4 is mobilized by neuronal activity to support the energetic demands of firing synapses. This mobilization relies on an AMP-kinase-mediated metabolic feedback to regulate GLUT4 delivery in nerve terminals similar to muscle. Finally, we show that acute genetic ablation of GLUT4 leads to an arrest of synaptic vesicle recycling, mimicking the deficits seen with glucose deprivation.

RESULTS

GLUT4 Is Expressed in the Brain and Is Present at Nerve Terminals

We verified previous reports of GLUT4 expression in both cerebellum (Kobayashi et al., 1996; Vannucci et al., 1998) and

hippocampus (Fernando et al., 2008; Grillo et al., 2009) using immunohistochemical staining with an anti-GLUT4 antibody in acute brain slices (Figure 1A–1D). GLUT4 is expressed throughout the hippocampus (Figure 1A), including layers enriched in presynaptic endings, such as stratum radiatum, as indicated by counterstaining against the SV marker VGLUT1 (Figure 1C). In the cerebellum, GLUT4 expression is pronounced in the granular layer, which contains soma, dendrites, and axons (Figure 1B), but appears to be lower in Purkinje cells (Figure 1D), consistent with previous observations (Vannucci et al., 1998). To further characterize the subcellular distribution of GLUT4 and determine if it is present in nerve terminals, we carried out immunocytochemistry analysis in dissociated rat hippocampal neurons which showed that GLUT4 is widely distributed throughout the soma and dendrites (Figure 1E) and additionally co-localizes with the abundant presynaptic protein synapsin (Figure 1F). Neurons in which GLUT4 was ablated (by small hairpin RNA [shRNA] expression) showed much lower levels of staining (Figures 1G and 1H), while neurons overexpressing GLUT4 were stained more brightly (Figures S1A and S1B) than the control, confirming the specificity of GLUT4 immunocytochemistry. Thus, we conclude that GLUT4 is distributed throughout neurons, including nerve terminals.

Activity Drives GLUT4 to the Presynaptic Plasma Membrane

We expressed a pHluorin-tagged variant of GLUT4 (Burchfield et al., 2013) in primary neurons (Figure S2A) to examine its behavior during action potential (AP) firing, which led to an ~2-fold overexpression of GLUT4 in nerve terminals (Figure S2B). Under resting conditions, pHluorin, which was spliced into the first exo-facial loop of GLUT4, is expected to be quenched if it resides in an acidic endosomal compartment. Rapid perfusion of a low pH solution that quenches surface pHluorin fluorescence showed that very little GLUT4-pHluorin (7.5% of total) resides on the axonal surface under resting conditions (Figures 2A and 2D). Perfusion with NH_4Cl at pH 7.4 rapidly equilibrates organelle pH to that of the buffer (Figures 2A, 2C, and S2A), demonstrating that GLUT4-pHluorin (GLUT4-pH) primarily resides in an acidic compartment. AP firing led to rapid accumulation of GLUT4 on the synaptic surface that persisted for ~2 min after the end of the stimulus (Figures 2B and 3C). We verified that the increased GLUT4-pH signal arose from surface accumulation, as it was fully quenched by perfusion of low-pH solution (Figure 2C). On average, persistent AP firing led to a maximal accumulation of ~20% of the total pool (i.e., the fluorescence achieved during a prior NH_4Cl perfusion) of GLUT4 on the synaptic surface of boutons (Figure 2D). The time constant of surface GLUT4 accumulation during constant AP firing was only approximately two times slower than SVs (data not shown), indicating that even a few APs likely recruit GLUT4 to the plasma membrane. Indeed, stimulation with 100 APs is sufficient to cause a statistically significant increase in GLUT4-pH fluorescence (Figure 2B, inset), but smaller fluorescence changes with fewer APs would be difficult to detect experimentally. Given previous reports of insulin-mediated regulation of neuronal GLUT4 (Fernando et al., 2008; Grillo et al., 2009), we examined the effects of insulin on GLUT4 trafficking in hippocampal axons. Consistent with the somatodendritic distribution of the insulin receptor (Abbott et al., 1999), acute insulin treatment failed to affect axonal surface GLUT4 levels (Figure S3A), while it did trigger surface accumulation of GLUT4 in somatodendritic compartments (data not shown). Similarly, long-term insulin deprivation did not impact activity-driven presynaptic GLUT4 mobilization (Figure S3B). Thus, like muscle contraction, presynaptic GLUT4 mobilization in response to activity is distinct from insulin signaling.

Although previous studies implied that the canonical neuronal glucose transporter GLUT3 redistributes to somatic and dendritic cell surface during prolonged activity (Ferreira et al., 2011), expression of a pHluorin-tagged GLUT3 (see STAR Methods) showed that under resting conditions, virtually all of the expressed GLUT3-pH was resident on the axonal surface, and AP firing led to no detectable increase in surface accumulation (Figures 2E–2G). Thus, in axons, GLUT3 likely provides a constant source of glucose uptake that is not significantly regulated by activity.

GLUT4 Recycling Is Distinct from Synaptic Vesicles

We wondered if the intracellular pool of GLUT4 vesicles is distinct from that of SVs. To examine this issue we used several approaches, including characterization of the both the biophysical properties of presynaptic GLUT4-pH (described here) and the molecular basis of the control of GLUT4-pH (described below). We previously developed methods to determine the pH inside organelles harboring pHluorin by monitoring the change in fluorescence resulting from rapid and reversible perfusion of NH_4Cl (Sankaranarayanan et al., 2000). Applying these approaches to GLUT4-pH in nerve terminals showed that the average pH of the endosomes harboring GLUT4 is ~6.1 (Figure 3A), more alkaline than typical SVs (~5.5) (Sankaranarayanan et al., 2000). The slow recovery of GLUT4-pH following stimulation (Figure 3B) also differs significantly from typical SV proteins, for which pHluorin-tagged variants are endocytosed and reacidified following exocytosis in ~6 s at 37°C (Balaji et al., 2008), indicating at the very least that they are likely recycled by different molecular mechanisms. Co-expression of GLUT4-pH and VGLUT1-mOrange2 (VGLUT1-mO) allowed us to examine the recycling behavior of the two proteins simultaneously after a stimulus. We found that GLUT4-pH recovers with a time for signal to decay by 50% ($t_{1/2}$) ~20 times slower that SVs (Figures 3B and 3C). Finally, the maximal fraction of GLUT4-pH driven to the surface by electrical activity (~20%, Figure 2D) is much smaller than that for SVs (~45%) (Kim and Ryan, 2010). These data all suggest that although GLUT4 is driven to undergo exocytosis at nerve terminals by AP firing, it likely does so from an endosomal compartment that is distinct from SVs.

GLUT4 Is Required for Sustained Synaptic Function

We tested the idea that insertion of GLUT4 during activity is critical for energetic support of SV endocytosis, which is blocked in the absence of stimulated glycolysis (Rangaraju et al., 2014). We examined the kinetics of SV recycling using VGLUT1-pH in neurons in which expression of *Glut4* was ablated using shRNA-mediated knockdown (KD) (Figures 1G, 1H, and S1B). We found that following co-expression of the shRNA targeting *Glut4* and VGLUT1-pH, resting ATP levels were not significantly changed

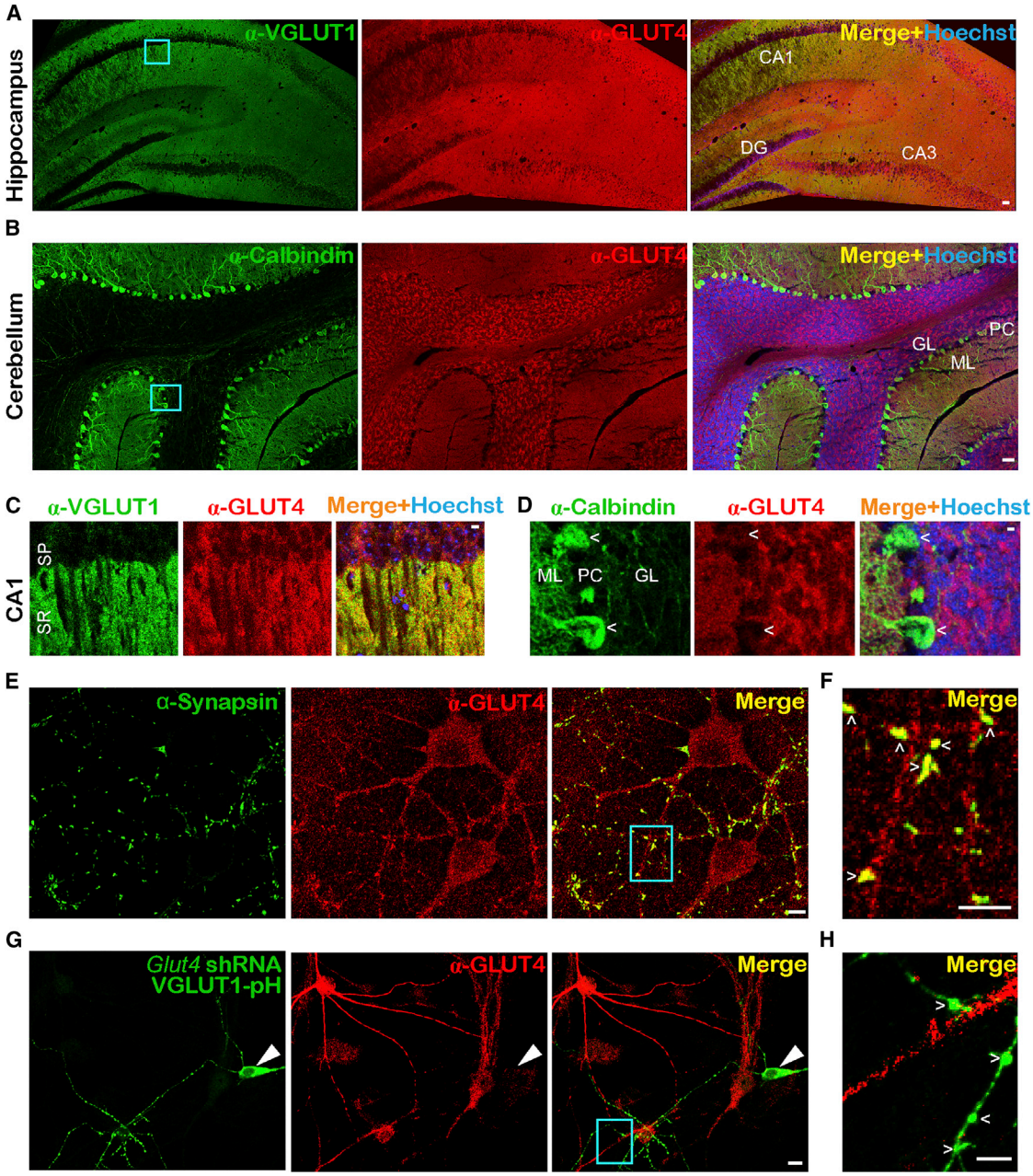

Figure 1. The Glucose Transporter GLUT4 Is Expressed in the Brain and Is Present at Nerve Terminals

(A–D) Immunohistochemical staining of adult mouse brain slices with antibodies against GLUT4 (red) and the presynaptic marker VGLUT1 (A and C) or the Purkinje cell marker calbindin (B and D) (green). Hoechst nuclear staining is shown in blue. Enlarged images of the cyan boxes in (A) and (B) show that GLUT4 is enriched in the synaptic-rich stratum radiatum (C) and expressed at lower levels in Purkinje cells (D, arrowheads). DG, dentate gyrus; GL, granule layer; ML, molecular layer; PC, Purkinje cells; SP, stratum pyramidale; SR, stratum radiatum. CA1 and CA3 are hippocampal regions.

(E–H) Immunostaining of dissociated rat hippocampal neurons with antibodies against GLUT4 (red) and (E and F) the presynaptic marker synapsin or (G and H) pHluorin/GFP of VGLUT1-pH (green) in neurons expressing *Glut4* shRNA. (E) GLUT4 is broadly expressed in somato-dendritic regions (F) but also co-localizes with synapsin at nerve terminals (arrowheads), as shown in the enlarged image of the cyan box in (D).

(G–H) GLUT4 immunofluorescence is reduced (by 70%, see STAR Methods) in neurons transfected with *Glut4* shRNA and VGLUT1-pH, indicating the specificity of GLUT4 antibody. Large arrowheads point to the soma (G), and small arrowheads point to boutons of the transfected neuron (H).

Scale bars represent 50 μm (A and B) or 5 μm (C–H). See also Figure S1.

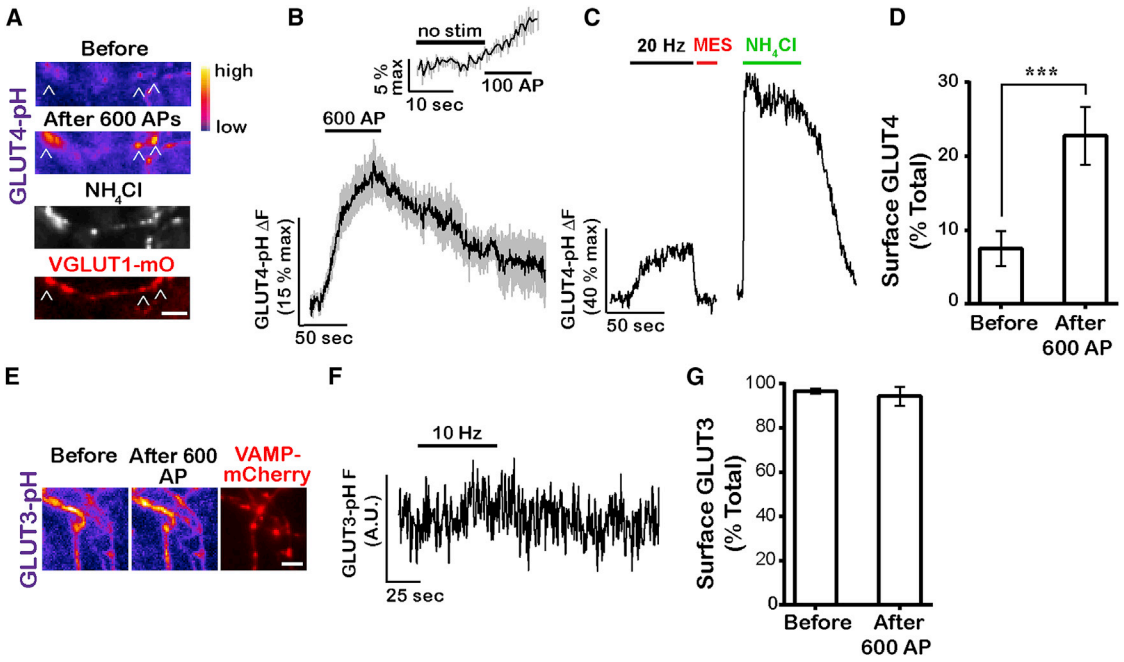

Figure 2. Neuronal Firing Drives GLUT4 Vesicles to the Presynaptic Plasma Membrane

(A–D) Neurons expressing GLUT4-pH were electrically stimulated with 600 APs. (A) GLUT4-pH (pseudocolor) and the synaptic vesicle marker VGLUT1-mO (red) before and after stimulation. Neutralization of GLUT4-pH vesicles with NH_4Cl (white) reveals total axonal pool. (B) Average trace of GLUT4-pH (n = 12 cells) with 600-AP stimulation with the inset showing response after the first 100 APs. ΔF values were normalized to maximal ΔF from NH_4Cl treatment. Error bars are shown in gray and represent SEM. (C) A sample trace where stimulation was followed by quenching of extracellular pHluorin with 2-ethanesulfonic acid (MES) acid and neutralization of GLUT4-pH vesicles with NH_4Cl. (D) Average surface fraction of GLUT4-pH before and after stimulation (% total; before, 7 ± 2; after 600 APs, 23 ± 4; n = 11 cells).

(E–G) GLUT3-pH does not mobilize at nerve terminals in response to activity. (E) Pseudocolor images of GLUT3-pH in axons co-expressing the synaptic vesicle marker VAMP-mCherry (red) before and after stimulation with 600 APs (10 Hz). (F) Sample trace of GLUT3-pH fluorescence (in arbitrary units) in response to stimulation. (G) Average surface fraction of GLUT3-pH before and after stimulation (% total; before, 97 ± 1; after 600 APs, 94 ± 5; n = 5 cells).

Scale bars in (A) and (E) represent 5 μm. All data are shown as mean ± SEM. See also Figures S2 and S3.

(Figure S4A). Approximately one-third of neurons (9/26) had a high resting fluorescence and no longer elicited any exocytic response (not shown). The remaining neurons had normal exocytosis in the absence of GLUT4 (Figures 4A and 4D) but showed a dramatic arrest of endocytosis and reacidification (Figures 4A and 4C). Perfusion of low-pH solution after AP firing (Figure 4B) indicated that virtually all of the elevated post-stimulus VGLUT1-pH fluorescence could be quenched, confirming that loss of GLUT4 in neurons leads to an arrest of SV endocytosis, a defect that is very similar to that observed following acute blockade of glycolysis (Rangaraju et al., 2014). Re-expressing an shRNA-insensitive variant of GLUT4 in KD neurons fully restored SV recycling (Figures 4A and 4C). It is possible that the requirement for GLUT4 in SV recycling is unrelated to its function as a glucose transporter. We tested this hypothesis by introducing a point mutation (E329Q) in a region of GLUT4 that is conserved between this transporter and GLUT1, in which this mutation inactivates the transport function, locking GLUT1

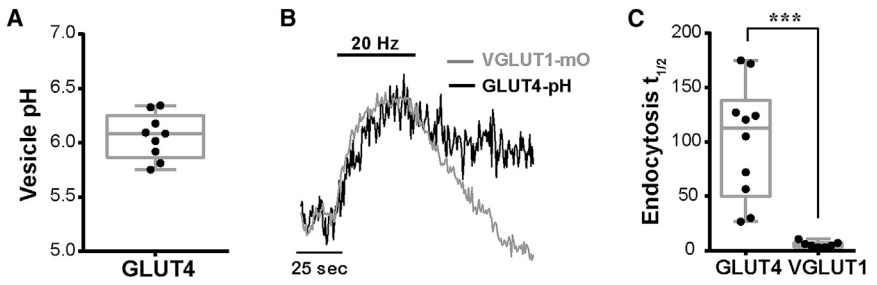

Figure 3. GLUT4 Vesicles Are Distinct from Synaptic Vesicles

(A) The pH of axonal GLUT4 vesicle measured from responses to acid quenching and neutralization with NH_4Cl. The box and whisker plot represents median (line), 25^{th}–75^{th} percentile (box), and min–max (whisker). Mean pH, 6.1 ± 0.1; n = 9 cells.

(B) Sample traces from boutons co-expressing GLUT4-pH and VGLUT1-mO stimulated with 600 APs (20 Hz).

(C) Decay half-time (seconds) of GLUT4-pH and VGLUT1-pH (in separate cells) after stimulation with 600 APs (10 Hz); GLUT4-pH, 101 ± 17; VGLUT1-pH, 6 ± 1; n = 7–10 cells per condition. ***p < 0.001.

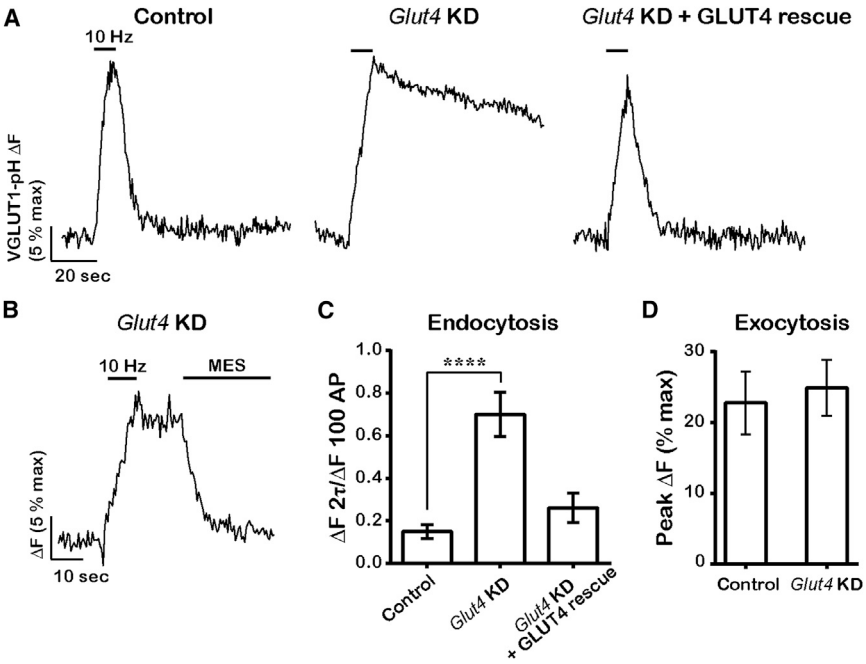

Figure 4. GLUT4 Is Required for Synaptic Vesicle Recycling following Bursts of AP Firing

(A–D) Sample VGLUT1-pH traces in response to 100 APs (10 Hz) in control, *Glut4* KD, and *Glut4* KD neurons expressing shRNA-resistant GLUT4-RFP (A) or in *Glut4* KD neurons (B), where stimulation was followed by quenching of extracellular pHluorin with MES acid. (C) Average endocytic block measured as the fraction of VGLUT1-pH signal remaining at two endocytic time constants (2τ) of the control at the end of stimulation. Control, 0.15 ± 0.03; *Glut4* KD, 0.7 ± 0.1; rescue, 0.26 ± 0.07; n = 13–17 cells. (D) Average exocytosis of VGLUT1-pH measured as ΔF at the end of 100 APs normalized to ΔF_{NH4Cl} (% max). Control, 23 ± 4; *Glut4* KD, 25 ± 4; n = 13–15 cells. All error bars represent SEM. ****p < 0.0001. See also Figure S4.

in an inward-facing conformation (Deng et al., 2014). The transport-deficient GLUT4-pHluorin showed very similar behavior to the wild-type form during AP firing, accumulating on the axonal presynaptic surface (Figures 5A and 5B). However, expression of transport-deficient GLUT4-RFP failed to rescue SV recycling in *Glut4* KD neurons (Figure 5C), even though this mutant was still able to rapidly insert into the plasma membrane during activity. Thus, the presence of a functional transporter on the synaptic surface is required for sustained SV recycling.

We wondered if this acute reliance on new glucose uptake would be mitigated during more modest levels of activity. Although endocytosis of SVs is blocked in dGlu following 100 AP stimuli, we found that the defect is much more modest for smaller numbers of stimuli (Figures 6A and 6C). Similar to full glycolytic block, we found that SV endocytosis was much more dramatically impacted in *Glut4* KD for stimuli of 100 APs compared to smaller stimuli (Figures 6B and 6C). These experiments reveal that in the absence of glycolysis, there is sufficient reserve ATP to handle a brief burst of activity but that synapses rely on the acute delivery of GLUT4 to the axonal surface to sustain function when more than approximately ten APs are fired in a short period of time.

AMP Kinase Mediates GLUT4 Mobilization during Activity

Exercise-driven mobilization of GLUT4 in muscle is driven by activation of AMP kinase (AMPK) as a result of a transient change in the AMP (or ADP) to ATP ratio (Fryer et al., 2002; Kurth-Kraczek et al., 1999; Mu et al., 2001), and this enzyme has also been shown to be activated in neurons by AP firing (Sample et al., 2015). We present three key pieces of evidence to support the

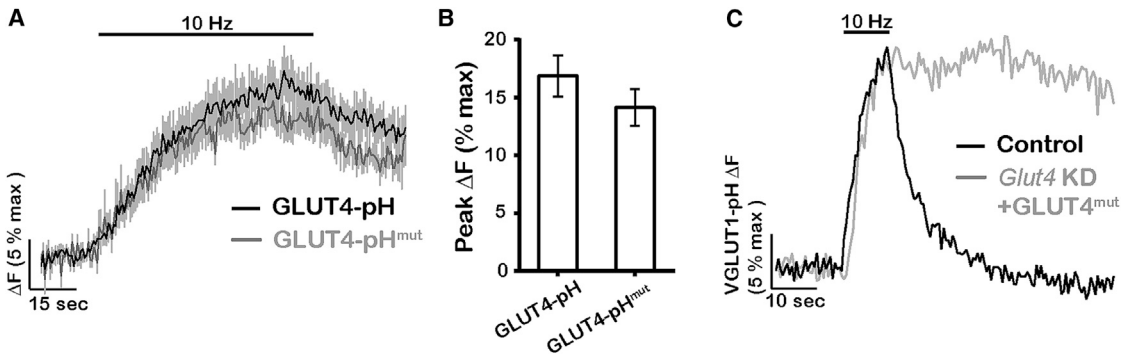

Figure 5. The Glucose Transport Activity of GLUT4 Is Essential for Synaptic Vesicle Recycling

(A and B) GLUT4 mutant defective in glucose transport is recruited to synaptic surface similar to wild-type. (A) Average traces of wild-type and mutant GLUT4-pH stimulated with 600 APs (10 Hz). Error bars are shown in gray. (B) Average peak ΔF of GLUT4-pH (% max) in response to 600 APs. Control data are the same as in Figure 2B. Control, 17 ± 2; GLUT4-pH^{mut}, 14 ± 2; n = 6–16 cells.

(C) Sample VGLUT1-pH traces in response to 100 APs (10 Hz) in control or *Glut4* KD neurons expressing shRNA-resistant GLUT4 mutant.

All error bars represent SEM.

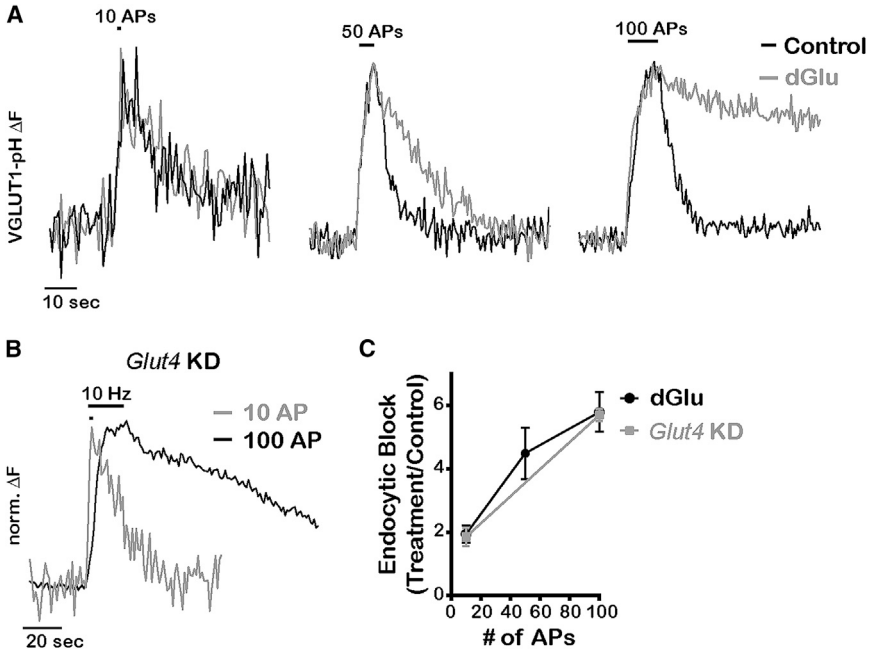

Figure 6. Energetic Requirement for Glycolysis and Glucose Uptake Increases with Duration of Activity

(A) Normalized VGLUT1-pH traces in response to 10, 50, and 100 APs (10 Hz) before and 5 min after incubation with dGlu.

(B) Normalized VGLUT1-pH traces of *Glut4* KD neurons stimulated with 10 or 100 APs (10 Hz).

(C) Average endocytic block for varying AP trains measured as the fraction of the maximal fluorescence remaining after two endocytic time constants in treated (dGlu or *Glut4* KD) compared to control conditions; n = 4–21 cells per condition. All error bars represent SEM.

idea that GLUT4 mobilization in axons is controlled by AMPK. First, we found that acute application of the AMPK activator 5-aminoimidazole-4-carboxamide ribonucleotide (AICAR) (Merrill et al., 1997) led to a rapid increase in GLUT4-pH signal in axons but did not trigger mobilization of SVs (Figure 7A, right). We verified that the increased GLUT4-pH signal was due surface accumulation of GLUT4 through exocytosis, as it was fully quenched by perfusion of low-pH solution (Figure 7A, left). Thus, activation of AMPK alone can drive GLUT4 exocytosis at nerve terminals from an internal endosomal compartment distinct from SVs. Second, in order to determine if an AMPK pathway is engaged during AP firing, we examined the impact of inhibiting AMPK on GLUT4 mobilization during electrical activity. Blockade of AMPK using the AMPK inhibitor dorsomorphin (Zhou et al., 2001) or expression of the catalytically inactive α subunit of AMPK (Woods et al., 2000) significantly reduced activity-driven GLUT4 translocation (Figures 7B and 7C). Dorsomorphin also blunted AICAR-mediated GLUT4 translocation (Figure S5A), validating its inhibitory effects on AMPK. In agreement with previous results in muscle (Mu et al., 2001), AMPK inhibition only partially blunted GLUT4 mobilization, suggesting that other regulatory factors, such as the elevation of intracellular calcium during activity, may also contribute to GLUT4 recruitment. Third, expression of a constitutively dephosphorylated form of the Rab GAP protein TBC1D1 (TBPC1D1-3A: S621, S231, and T499 mutated to alanine), a critical target of AMPK that regulates GLUT4 translocation in muscle (Vichaiwong et al., 2010), significantly slowed activity-driven exocytosis of GLUT4 at nerve terminals (Figures 7D and 7E). In contrast, expression of AS160, an adipocyte isoform of TBC1D1 in which Akt phosphorylation sites downstream of insulin signaling were mutated (Sano et al., 2003), did not affect activity-driven GLUT4 trafficking (data not shown). These data together support the idea that activation of the metabolic sensor AMPK is the primary driver of GLUT4 exocytosis at nerve terminals. AMPK does not, however, regulate SV exocytosis, as neither dorsomorphin nor TBC1D1-3A had any impact on exocytosis of VGLUT1-pH (Figures S5D and S5E), despite their inhibitory effects on GLUT4 mobilization. Given the arrest of SV recycling in *Glut4* KD neurons (Figure 4), we reasoned that blunting AMPK-driven GLUT4 translocation would similarly slow SV endocytosis for large stimuli. Although dorsomorphin treatment or TBC1D1-3A expression alone only partially impaired GLUT4 translocation (Figures 7B–7E), when combined, their affects were additive (Figures S5B and S5C). Under these conditions, SV endocytosis following a large stimulus slowed significantly (Figure 7F). Thus, we conclude that AMPK-driven GLUT4 exocytosis is essential for proper synaptic function.

GLUT4 and Synaptic Vesicles Use Distinct Pathways of Exocytosis

Our finding that AMPK specifically drives exocytosis of GLUT4 vesicles, but not SVs (Figure 7), suggests that GLUT4 and SVs may use distinct exocytic machinery. To address this, we examined the effects of known blockers of SV exocytosis on GLUT4 trafficking. An important consideration, however, in examining the molecular basis of GLUT4 exocytosis is that perturbations that impact SV cycling might lessen the activation of AMPK, since SV recycling is one of the major consumers of ATP in nerve terminals (Rangaraju et al., 2014). We therefore examined both how a given molecular regulator impacts electrical-activity-driven and AICAR-driven GLUT4 exocytosis. First, we expressed the tetanus-toxin light chain (TeNT-LC) to cleave the SNARE protein VAMP2 that fully eliminates SV exocytosis (Gaisano et al., 1994) and found that GLUT4 mobilization by electrical activity and AICAR were similarly blocked (Figures 8A and 8C). Therefore, consistent with previous findings in muscle (Randhawa et al., 2000), VAMP2 is required for presynaptic GLUT4 exocytosis. Second, we used shRNA to ablate the expression of *Munc13*, a SNARE-associated protein required for both evoked and spontaneous SV release (Varoqueaux et al., 2002), to completely block SV exocytosis (Figure S6A). In contrast to SVs, activity-driven mobilization of GLUT4 persisted, albeit at lower levels, in *Munc13* KD neurons (Figures 8B and 8C). Significantly, exocytosis of GLUT4 in response to AICAR was

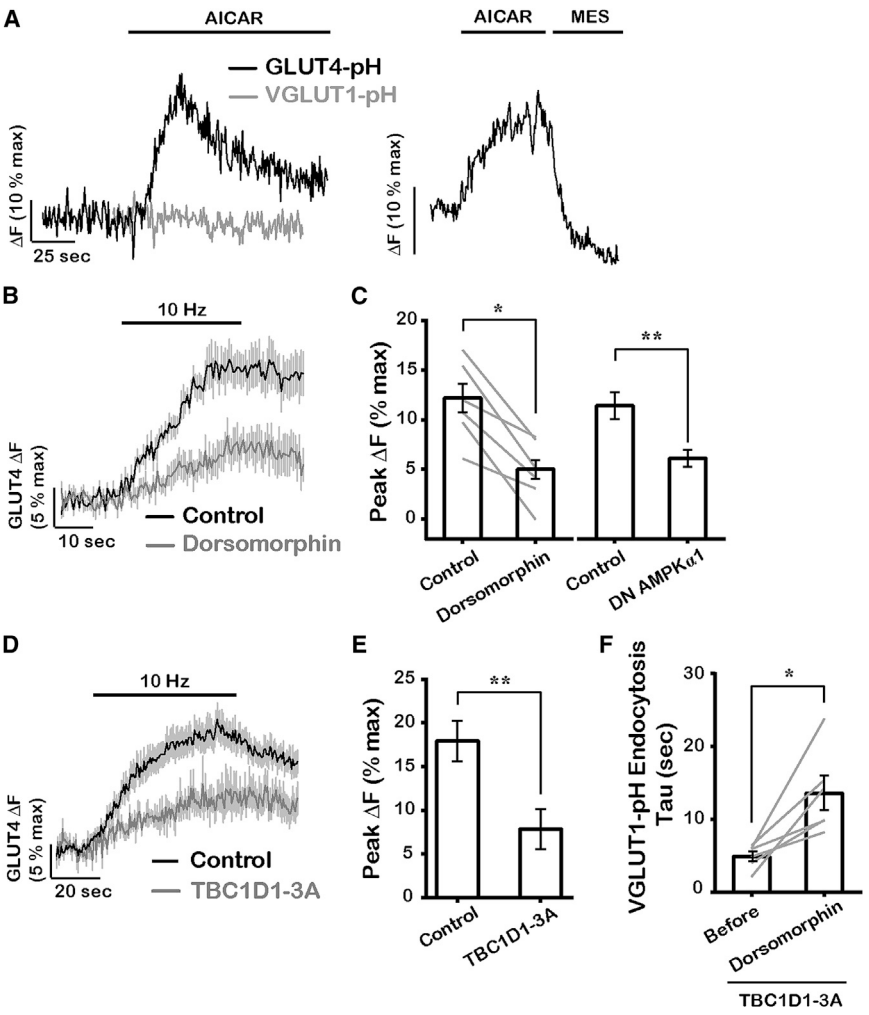

Figure 7. AMP Kinase Mediates Mobilization of GLUT4 at Presynaptic Boutons

(A) Representative responses of GLUT4-pH and VGLUT1-pH to treatment with 1 mM AICAR (left) or AICAR treatment of GLUT4-pH (right) immediately followed by MES acid quench.

(B) Average traces of GLUT4-pH stimulated with 300 APs (10 Hz) before and 25 min after incubation with 10 μM dorsomorphin, an AMPK inhibitor.

(C) Average GLUT4 peak ΔF (% max) in response to 300 APs before and after dorsomorphin treatment or 600 APs with or without expression of dominant-negative (DN) AMPKα1. Due to the reduction of ΔF_{max} values with the expression of DN AMPKα1, all ΔF_{max} values were normalized to the control (see STAR Methods). Control, 12 ± 1; dorsomorphin, 5 ± 1; control, 11 ± 1; DN AMPKα1, 5.9 ± 0.8; n = 6–8 cells.

(D) Average GLUT4-pH traces in response to 600 APs (10 Hz) in control neurons or neurons expressing TBC1D1-3A in which putative AMPK phosphorylation sites were mutated.

(E) Average maximal ΔF (% max) in response to 600 APs in control and TBC1D1-3A-expressing neurons. Control data are the same as in Figure 2B. Control, 18 ± 2; TBC1D1-3A, 8 ± 2; n = 8–12 cells.

(F) Endocytosis time constant (seconds) of VGLUT1-pH in neurons expressing TBC1D1-3A, stimulated with 600 APs (10 Hz) before and after 30 min of dorsomorphin treatment. Before, 4.9 ± 0.7; dorsomorphin, 14 ± 2; n = 6 cells.

Error bars in graphs are shown in gray (B and D). All error bars represent SEM. *p < 0.05, **p < 0.01. See also Figure S5.

completely unaffected by MUNC13 removal (Figures 8B and 8C), indicating that GLUT4 vesicles, unlike SVs, do not require MUNC13 for exocytosis. We attribute the decrease in GLUT4 mobilization in firing *Munc13* KD neurons to the reduced energy burden in these neurons, as elimination of SV cycling significantly lowers ATP consumption and, consequently, AMPK activation during activity. It is interesting to note that the earliest phase of AP-driven exocytosis of GLUT4 is not altered by the absence of MUNC13, suggesting that the initial trigger for exocytosis is not AMPK driven or that some other transient energy burden associated with electrical activity drives the early phase of GLUT4 insertion. Overall, these findings demonstrate that GLUT4 and SVs utilize distinct pathways for exocytosis during neuronal firing and, taken together with the different recycling kinetics (Figure 3), strongly support the idea that in nerve terminals, GLUT4 does not reside in SVs.

DISCUSSION

Our data reveal a new and important principle of metabolic regulation of presynaptic function: similar to exercising muscle, "exercising" axons also rely on translocation of the GLUT4 glucose transporter to the plasma membrane for metabolic homeostasis. While previous studies investigated potential regulation of neuronal GLUT4 by insulin (Fernando et al., 2008; Grillo et al., 2009), we uncovered a novel metabolic role for GLUT4 at synapses that more closely resembles its function in muscle than adipocytes. We also show that like muscle, activity-driven mobilization of GLUT4 at synapses is distinct from activation of insulin signaling. In the future, it will be interesting to examine how insulin affects GLUT4 trafficking in soma and dendrites and how GLUT4 in turn may regulate post-synaptic function. Similar to neurons, membrane depolarization in muscle, even in the absence of contraction, can drive GLUT4 mobilization (Wijesekara et al., 2006), suggesting that in both systems, electrical stimulation may be sufficient for AMPK activation.

At present, the identity and molecular composition of presynaptic GLUT4 vesicles remains unknown, but four types of experiments strongly suggest that they are distinct from synaptic vesicles. First, the average pH of the presynaptic GLUT4-bearing compartment is more alkaline than that of SVs (Figure 3A). Second, following exocytosis, GLUT4 endocytosis proceeds more slowly than SVs (Figures 3B and 3C). Third, although direct activation of AMPK drives GLUT4 exocytosis, it does not induce SV exocytosis (Figure 7A). Fourth, unlike its requirement for SVs, exocytosis of GLUT4 vesicles does not rely on MUNC13 (Figures 8B and 8C).

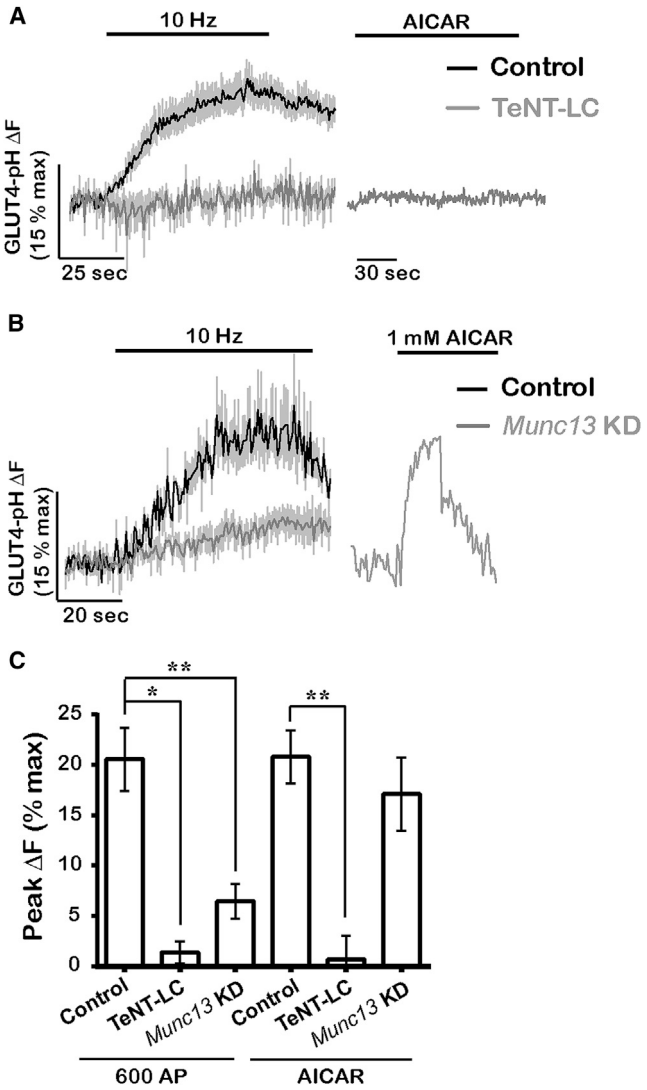

Figure 8. GLUT4 and Synaptic Vesicles Use Distinct Machinery for Exocytosis

(A) Expression of tetanus toxin light chain (TeNT-LC) blocks GLUT4 exocytosis in response to electrical stimulation (600 APs, 10 Hz) and AICAR treatment.

(B) *Munc13* KD does not block AICAR-driven GLUT4 exocytosis while it only partially inhibits activity-driven exocytosis (600 APs, 10 Hz).

(C) Average peak ΔF (% max) in response to 600 APs or AICAR in the same genotypes as shown in (A) and (B). 600 APs (control, 20 ± 3; TeNT-LC, 1 ± 1; *Munc13* KD, 6 ± 2); AICAR (control, 20 ± 3; TeNT-LC, 0 ± 2; *Munc13* KD, 17 ± 4); n = 3–13 cells.

Error bars in graphs are shown in gray (A and B). All error bars represent SEM. See also Figure S6.

Together, these results strongly argue that the activity-regulated GLUT4 vesicle pool is distinct from that of SVs.

As a regulatory module, the extent of GLUT4 mobilization in boutons is expected to match their energetic needs through a feedback mechanism involving AMPK. Indeed, GLUT4 surface recruitment was diminished in *Munc13* KD neurons in which the energetic burden of SV recycling was eliminated (Figures 8B and 8C). In contrast, activity-driven membrane recruitment of the transport deficient GLUT4 mutant was not elevated compared to the control (Figures 5A and 5B), even though the energetic demands of SV recycling were not met by this mutant (Figure 5C). This apparent lack of a feedback loop in the latter case may be due to the limited amount of GLUT4 available for recycling (~20%) that is already maximally mobilized in control conditions during our stimulation paradigm (600 APs, 10 Hz).

Our findings imply that the requirement of GLUT4 mobilization is not evident under modest stimulation conditions. Instead, it is a mechanism that is required for sustained function under constant firing, presumably a condition that engages sufficient metabolic imbalance to activate AMPK. Although GLUT4 knockout animals survive to adulthood, they suffer from numerous physiological abnormalities, including shortened lifespan (Katz et al., 1995). The consequences of GLUT4 ablation on neuronal network function has yet to be assessed, but given the importance of fuel availability for brain function, removal of one pathway is likely compensated by other metabolic pathways. Indeed, loss of GLUT4 in cardiac tissue, an organ that requires constant fuel supply, leads to upregulation of GLUT1, which only over time results in the development of cardiac hypertrophy (Abel et al., 1999). Our experiments predict that in the absence of any such compensation, loss of GLUT4 in the brain would primarily impact circuits that rely on sustained (many seconds) of activity. It is interesting to note that a poorly understood but effective treatment for drug-resistant childhood epilepsy relies on nutrient supply from a diet that heavily favors ketogenic rather than glycolytic metabolism (Neal et al., 2008). Given that seizure propagation requires sustained neuronal firing with a heavy reliance on activity-driven glycolysis, it is tempting to speculate that the mechanism of protection offered by ketogenic diets is to dampen circuit activity by allowing a block of vesicle recycling. Our findings demonstrate that a critical metabolic regulatory module that supports muscle function during acute changes in demand is operational at nerve terminals, potentially opening up new routes for therapeutic intervention.

STAR★METHODS

Detailed methods are provided in the online version of this paper and include the following:

- KEY RESOURCES TABLE
- CONTACT FOR REAGENT AND RESOURCE SHARING
- EXPERIMENTAL MODEL AND SUBJECT DETAILS
  - Animals
  - Primary Neuronal Culture
- METHOD DETAILS
  - Plasmid Constructs
  - Live Imaging of Neurons
  - GLUT4-pH Measurements
  - Brain Slice Immunohistochemistry
  - Dissociated Neuron Immunocytochemistry
  - Validation of *Glut4* Knockdown by Immunostaining
- QUANTIFICATION AND STATISTICAL ANALYSIS
  - Image Analysis and Statistics
  - Quantification of Synaptic Vesicle Endocytic Block

SUPPLEMENTAL INFORMATION

Supplemental Information includes six figures and can be found with this article online at http://dx.doi.org/10.1016/j.neuron.2016.12.020.

AUTHOR CONTRIBUTIONS

T.A.R. and G.A. designed the study. G.A. performed the experiments, with the exception of brain slice immunostaining, which was carried out by Z.W. and R.J.F. in the laboratory of Marc Tessier Lavigne (Rockefeller University). T.A.R. and G.A. wrote the manuscript.

ACKNOWLEDGMENTS

We thank members of the T.A.R. laboratory, Jeremy Dittman, and Tim McGraw for their valuable suggestions and input on this work. We thank David James (University of Sydney) for providing us with the GLUT4-pH construct, Gus Leinhard (Dartmouth University) for the TBC1D1 construct, and G. Bell (University of Chicago) for the GLUT3 construct. This work was supported by a grant to T.A.R. from the NIH (NS036942).

Received: September 6, 2016
Revised: November 8, 2016
Accepted: December 15, 2016
Published: January 19, 2017

REFERENCES

Abbott, M.A., Wells, D.G., and Fallon, J.R. (1999). The insulin receptor tyrosine kinase substrate p58/53 and the insulin receptor are components of CNS synapses. J. Neurosci. *19*, 7300–7308.

Abel, E.D., Kaulbach, H.C., Tian, R., Hopkins, J.C., Duffy, J., Doetschman, T., Minnemann, T., Boers, M.E., Hadro, E., Oberste-Berghaus, C., et al. (1999). Cardiac hypertrophy with preserved contractile function after selective deletion of GLUT4 from the heart. J. Clin. Invest. *104*, 1703–1714.

Balaji, J., and Ryan, T.A. (2007). Single-vesicle imaging reveals that synaptic vesicle exocytosis and endocytosis are coupled by a single stochastic mode. Proc. Natl. Acad. Sci. USA *104*, 20576–20581.

Balaji, J., Armbruster, M., and Ryan, T.A. (2008). Calcium control of endocytic capacity at a CNS synapse. J. Neurosci. *28*, 6742–6749.

Burchfield, J.G., Lu, J., Fazakerley, D.J., Tan, S.X., Ng, Y., Mele, K., Buckley, M.J., Han, W., Hughes, W.E., and James, D.E. (2013). Novel systems for dynamically assessing insulin action in live cells reveals heterogeneity in the insulin response. Traffic *14*, 259–273.

Chauveau, M.A., and Kaufmann, M. (1887). Experiences pour la determination du coefficient de l'activite nutritive et repiratoire des muscles en repos et en travail. C. R. Acad. Sci. *104*, 1126–1132.

Chow, B.Y., Han, X., Dobry, A.S., Qian, X., Chuong, A.S., Li, M., Henninger, M.A., Belfort, G.M., Lin, Y., Monahan, P.E., and Boyden, E.S. (2010). High-performance genetically targetable optical neural silencing by light-driven proton pumps. Nature *463*, 98–102.

Deng, D., Xu, C., Sun, P., Wu, J., Yan, C., Hu, M., and Yan, N. (2014). Crystal structure of the human glucose transporter GLUT1. Nature *510*, 121–125.

Douen, A.G., Ramlal, T., Rastogi, S., Bilan, P.J., Cartee, G.D., Vranic, M., Holloszy, J.O., and Klip, A. (1990). Exercise induces recruitment of the "insulin-responsive glucose transporter". Evidence for distinct intracellular insulin- and exercise-recruitable transporter pools in skeletal muscle. J. Biol. Chem. *265*, 13427–13430.

Fernando, R.N., Albiston, A.L., and Chai, S.Y. (2008). The insulin-regulated aminopeptidase IRAP is colocalised with GLUT4 in the mouse hippocampus–potential role in modulation of glucose uptake in neurones? Eur. J. Neurosci. *28*, 588–598.

Ferreira, J.M., Burnett, A.L., and Rameau, G.A. (2011). Activity-dependent regulation of surface glucose transporter-3. J. Neurosci. *31*, 1991–1999.

Fryer, L.G., Foufelle, F., Barnes, K., Baldwin, S.A., Woods, A., and Carling, D. (2002). Characterization of the role of the AMP-activated protein kinase in the stimulation of glucose transport in skeletal muscle cells. Biochem. J. *363*, 167–174.

Gaisano, H.Y., Sheu, L., Foskett, J.K., and Trimble, W.S. (1994). Tetanus toxin light chain cleaves a vesicle-associated membrane protein (VAMP) isoform 2 in rat pancreatic zymogen granules and inhibits enzyme secretion. J. Biol. Chem. *269*, 17062–17066.

Gerhart, D.Z., Broderius, M.A., Borson, N.D., and Drewes, L.R. (1992). Neurons and microvessels express the brain glucose transporter protein GLUT3. Proc. Natl. Acad. Sci. USA *89*, 733–737.

Grillo, C.A., Piroli, G.G., Hendry, R.M., and Reagan, L.P. (2009). Insulin-stimulated translocation of GLUT4 to the plasma membrane in rat hippocampus is PI3-kinase dependent. Brain Res. *1296*, 35–45.

Hoppa, M.B., Lana, B., Margas, W., Dolphin, A.C., and Ryan, T.A. (2012). $\alpha 2\delta$ expression sets presynaptic calcium channel abundance and release probability. Nature *486*, 122–125.

Ikemoto, A., Bole, D.G., and Ueda, T. (2003). Glycolysis and glutamate accumulation into synaptic vesicles. Role of glyceraldehyde phosphate dehydrogenase and 3-phosphoglycerate kinase. J. Biol. Chem. *278*, 5929–5940.

Jang, S., Nelson, J.C., Bend, E.G., Rodríguez-Laureano, L., Tueros, F.G., Cartagenova, L., Underwood, K., Jorgensen, E.M., and Colón-Ramos, D.A. (2016). Glycolytic enzymes localize to synapses under energy stress to support synaptic function. Neuron *90*, 278–291.

Katz, E.B., Stenbit, A.E., Hatton, K., DePinho, R., and Charron, M.J. (1995). Cardiac and adipose tissue abnormalities but not diabetes in mice deficient in GLUT4. Nature *377*, 151–155.

Kim, S.H., and Ryan, T.A. (2010). CDK5 serves as a major control point in neurotransmitter release. Neuron *67*, 797–809.

Kimura, S., Noda, T., and Yoshimori, T. (2007). Dissection of the autophagosome maturation process by a novel reporter protein, tandem fluorescent-tagged LC3. Autophagy *3*, 452–460.

Knull, H.R., and Fillmore, S.J. (1985). Glycolytic enzyme levels in synaptosomes. Comp. Biochem. Physiol. B *81*, 349–351.

Kobayashi, M., Nikami, H., Morimatsu, M., and Saito, M. (1996). Expression and localization of insulin-regulatable glucose transporter (GLUT4) in rat brain. Neurosci. Lett. *213*, 103–106.

Kurth-Kraczek, E.J., Hirshman, M.F., Goodyear, L.J., and Winder, W.W. (1999). 5′ AMP-activated protein kinase activation causes GLUT4 translocation in skeletal muscle. Diabetes *48*, 1667–1671.

Lauritzen, H.P., Galbo, H., Toyoda, T., and Goodyear, L.J. (2010). Kinetics of contraction-induced GLUT4 translocation in skeletal muscle fibers from living mice. Diabetes *59*, 2134–2144.

Merrill, G.F., Kurth, E.J., Hardie, D.G., and Winder, W.W. (1997). AICA riboside increases AMP-activated protein kinase, fatty acid oxidation, and glucose uptake in rat muscle. Am. J. Physiol. *273*, E1107–E1112.

Mu, J., Brozinick, J.T., Jr., Valladares, O., Bucan, M., and Birnbaum, M.J. (2001). A role for AMP-activated protein kinase in contraction- and hypoxia-regulated glucose transport in skeletal muscle. Mol. Cell *7*, 1085–1094.

Neal, E.G., Chaffe, H., Schwartz, R.H., Lawson, M.S., Edwards, N., Fitzsimmons, G., Whitney, A., and Cross, J.H. (2008). The ketogenic diet for the treatment of childhood epilepsy: a randomised controlled trial. Lancet Neurol. *7*, 500–506.

Randhawa, V.K., Bilan, P.J., Khayat, Z.A., Daneman, N., Liu, Z., Ramlal, T., Volchuk, A., Peng, X.R., Coppola, T., Regazzi, R., et al. (2000). VAMP2, but not VAMP3/cellubrevin, mediates insulin-dependent incorporation of GLUT4 into the plasma membrane of L6 myoblasts. Mol. Biol. Cell *11*, 2403–2417.

Rangaraju, V., Calloway, N., and Ryan, T.A. (2014). Activity-driven local ATP synthesis is required for synaptic function. Cell *156*, 825–835.

Roy, D., and Marette, A. (1996). Exercise induces the translocation of GLUT4 to transverse tubules from an intracellular pool in rat skeletal muscle. Biochem. Biophys. Res. Commun. *223*, 147–152.

Ryan, T.A. (1999). Inhibitors of myosin light chain kinase block synaptic vesicle pool mobilization during action potential firing. J. Neurosci. *19*, 1317–1323.

Sample, V., Ramamurthy, S., Gorshkov, K., Ronnett, G.V., and Zhang, J. (2015). Polarized activities of AMPK and BRSK in primary hippocampal neurons. Mol. Biol. Cell *26*, 1935–1946.

Sankaranarayanan, S., De Angelis, D., Rothman, J.E., and Ryan, T.A. (2000). The use of pHluorins for optical measurements of presynaptic activity. Biophys. J. *79*, 2199–2208.

Sano, H., Kane, S., Sano, E., Mîinea, C.P., Asara, J.M., Lane, W.S., Garner, C.W., and Lienhard, G.E. (2003). Insulin-stimulated phosphorylation of a Rab GTPase-activating protein regulates GLUT4 translocation. J. Biol. Chem. *278*, 14599–14602.

Vannucci, S.J., Koehler-Stec, E.M., Li, K., Reynolds, T.H., Clark, R., and Simpson, I.A. (1998). GLUT4 glucose transporter expression in rodent brain: effect of diabetes. Brain Res. *797*, 1–11.

Varoqueaux, F., Sigler, A., Rhee, J.S., Brose, N., Enk, C., Reim, K., and Rosenmund, C. (2002). Total arrest of spontaneous and evoked synaptic transmission but normal synaptogenesis in the absence of Munc13-mediated vesicle priming. Proc. Natl. Acad. Sci. USA *99*, 9037–9042.

Vichaiwong, K., Purohit, S., An, D., Toyoda, T., Jessen, N., Hirshman, M.F., and Goodyear, L.J. (2010). Contraction regulates site-specific phosphorylation of TBC1D1 in skeletal muscle. Biochem. J. *431*, 311–320.

Voglmaier, S.M., Kam, K., Yang, H., Fortin, D.L., Hua, Z., Nicoll, R.A., and Edwards, R.H. (2006). Distinct endocytic pathways control the rate and extent of synaptic vesicle protein recycling. Neuron *51*, 71–84.

Wijesekara, N., Tung, A., Thong, F., and Klip, A. (2006). Muscle cell depolarization induces a gain in surface GLUT4 via reduced endocytosis independently of AMPK. Am. J. Physiol. Endocrinol. Metab. *290*, E1276–E1286.

Woods, A., Azzout-Marniche, D., Foretz, M., Stein, S.C., Lemarchand, P., Ferré, P., Foufelle, F., and Carling, D. (2000). Characterization of the role of AMP-activated protein kinase in the regulation of glucose-activated gene expression using constitutively active and dominant negative forms of the kinase. Mol. Cell. Biol. *20*, 6704–6711.

Zhou, G., Myers, R., Li, Y., Chen, Y., Shen, X., Fenyk-Melody, J., Wu, M., Ventre, J., Doebber, T., Fujii, N., et al. (2001). Role of AMP-activated protein kinase in mechanism of metformin action. J. Clin. Invest. *108*, 1167–1174.

STAR★METHODS

KEY RESOURCES TABLE

REAGENT or RESOURCE	SOURCE	IDENTIFIER
Antibodies		
Rabbit anti-GLUT4 antibody	Alomone Labs	CAT#: AGT-024, RRID: AB_2631197
Guinea pig anti-Synapsin 1/2	Synaptic Systems	CAT#: 106-004, RRID: AB_1106784
Chicken anti-GFP antibody	ThermoFisher Scientific	CAT#: A10263, RRID: AB_2534024
Guinea pig anti-VGLUT1	Millipore	CAT#: AB5905, RRID: AB_2301751
mouse anti-Calbindin	SWANT	CAT#: C9638, RRID: AB_2314070
Chemicals, Peptides, and Recombinant Proteins		
5-Aminoimidazole-4-carboxamide ribonucleotide (AICAR)	Abcam Biochemicals	CAT#: ab120358
Dorsomorphin	Sigma-Aldrich	CAT#: 866405-64-3
insulin-free B27	ThermoFisher Scientific	CAT#:A1895601
Critical Commercial Assays		
QuickChange site-directed mutagenesis kit	Agilent Technologies	CAT#: 210518
Experimental Models: Organisms/Strains		
Sprague-Dawley Rat	Charles River	Strain code: 400, RRID: RGD_734476
Recombinant DNA		
VGLUT1-pHluorin	Voglmaier et al., 2006	N/A
VGLUT1-mOrange2	Hoppa et al., 2012	N/A
MUNC13-1/2 shRNA	Rangaraju et al., 2014	N/A
TeNT-LC	Gift of M. Dong	N/A
GLUT4-pHluorin	Burchfield et al., 2013	N/A
GLUT4-RFP	This paper	N/A
GLUT4^{E329Q}-RFP	This paper	N/A
AMPKα1^{D159A}	This paper	N/A
TBC1D1-3A	This paper	N/A
GLUT3-pH	This paper	N/A
Syn-ATP	Rangaraju et al., 2014	N/A
Sequence-Based Reagents		
GLUT4-shRNA	OriGene Technologies	CAT#: TR709372A
Software and Algorithms		
ImageJ	National Institute of Health	https://imagej.nih.gov/ij/
GraphPad Prism 6.0	GraphPad Software	http://www.graphpad.com/scientific-software/prism/
OriginPro 8	OriginLab	http://www.originlab.com/

CONTACT FOR REAGENT AND RESOURCE SHARING

Further information and requests for resources and reagents should be directed to and will be fulfilled by the Lead Contact Timothy A. Ryan at taryan@med.cornell.edu.

EXPERIMENTAL MODEL AND SUBJECT DETAILS

Animals

All animal-related experiments were performed in accordance with protocols approved by the Weill Cornell Medicine or Rockefeller University IACUC. Wild-type rats and mice were of the Sprague-Dawley strain (Charles River code 400, RRID: RGD_734476), and CD1 background, respectively.

Primary Neuronal Culture

Hippocampal CA1-CA3 neurons were isolated from 1- to 3-day-old rats of mixed gender, plated on poly-ornithine-coated coverslips, transfected 7 days after plating, and imaged 14-21 days after plating as previously described (Ryan, 1999). Neurons were maintained in culture media composed of MEM (Thermo Fisher Scientific S1200038), 0.6% glucose, 0.1 g/l bovine transferrin (Millipore 616420), 0.25 g/l insulin, 0.3 g/l glutamine, 5%–10% fetal bovine serum (Atlanta Biologicals S11510), 2% B-27 (Thermo Fisher Scientific 17504-044), and 4 μm cytosine β-d-arabinofuranoside. Cultures were incubated at 37°C in a 95% air/5% CO2 humidified incubator for 14–21 days prior to use.

METHOD DETAILS

Plasmid Constructs

The following previously published DNA constructs were used: VGLUT1-pHluorin (Voglmaier et al., 2006), VGLUT1-mOrange2 (Hoppa et al., 2012), and VAMP-mCherry (Hoppa et al., 2012), *Munc13*-1/2 shRNA and Syn-ATP (Rangaraju et al., 2014), and TeNT-LC (gift of M. Dong). GLUT4-pHluorin was a gift from D. E. James (Burchfield et al., 2013). To construct GLUT4-RFP, HA-GLUT4 sequence was PCR first amplified from an HA-GLUT4-GFP plasmid (gift of T. E. McGraw) and inserted into the Bam H1 and Age1 sites of FCK-Arch –GFP (Chow et al., 2010), a gift of Edward Boyden (Addgene 22217), to replace Arch. mRFP was PCR amplified from pmRFP-LC3 (Kimura et al., 2007), a gift from Tamotsu Yoshimori (Addgene 21075), and inserted into EcoRI and AgeI sites of GLUT4-eGFP. The transport-deficient GLUT4-RFP was generated based on the structure of GLUT1 (Deng et al., 2014), where E329Q mutation in a region conserved between GLUT1 and GLUT4 locks the transporter in an inward-facing conformation. Mutagenesis was performed with the QuickChange site-directed mutagenesis kit (Stratagene, Agilent Technologies). Similarly, AMPKα1, a gift from Morris Birnbaum (Addgene 27297) was used for site-directed mutagenesis to generate dominant negative AMPKα1 (D159A). AMPK phosphorylation sites (S237, T505, and S627) (Vichaiwong et al., 2010) in TBC1D1 (gift of G. E. Leinhard) were mutated to alanine using Gibson assembly (New England Biolabs).

To construct GLUT3-pH, pHluorin sequence of VGLUT1-pH was PCR amplified along with the linker sequence encoding SGSTSGGSGGTG and inserted into the first extracellular loop of human GLUT3 (gift of G. Bell) between amino acids 50/51 using Gibson assembly. The resultant GLUT3-pH piece was PCR amplified and inserted into BamH1 and EcoRI sites of FCK-Arch –GFP. The shRNA targeting rat GLUT4 (TR709372A) was purchased from OriGene Technologies.

Live Imaging of Neurons

Unless otherwise indicated, all imaging experiments were performed on a custom-built laser illuminated epifluorescence microscope with an Andor iXon+ camera (model #DU-897E-BV). Acousto-optic tunable filters were used to shutter solid state 488 nm and 532 nm lasers. Images were acquired through a 40 X 1.3 NA Fluar Zeiss objective. Luminescence imaging of the presynaptic ATP reporter, Syn-ATP, was performed as previously described (Rangaraju et al., 2014). Coverslips were mounted in a laminar flow perfusion chamber and perfused at 37°C with Tyrodes buffer containing (in mM) 119 NaCl, 2.5 KCl, 2 $CaCl_2$, 2 $MgCl_2$, 50 HEPES (pH 7.4), 5 glucose, supplemented with 10 μM 6-cyano-7nitroquinoxalibe-2, 3-dione (CNQX), and 50 μM D,L-2-amino-5phosphonovaleric acid (APV) (both from Sigma) to suppress post-synaptic responses. Action potentials were evoked in neurons with 1 ms pulses creating field potentials of ~10 V/cm via platinum–iridium electrodes.

In deoxyglucose experiments, glucose in the Tyrodes buffer was replaced with 5 mM deoxyglucose. NH_4Cl solution for alkalization of pHluorin-containing vesicles had a similar composition as Tyrodes buffer except it contained (in mM): 50 NH_4Cl and 69 NaCl. The MES solution for acid quench of pHluorin, contained MES in place of HEPES and was set to pH 5.5. Insulin deprivation prior to acute insulin treatment or electrical stimulation was achieved by culturing neurons at days after plating 14-16 for 24-48 hr with media containing insulin-free B27 (ThermoFisher Scientific A1895601).

5-Aminoimidazole-4-carboxamide ribonucleotide (AICAR) purchased from Abcam Biochemicals, and dorsomorphin (compound C) purchased from Sigma-Aldrich, were diluted in Tyrodes buffer to 1 mM and 10 μM, respectively, and applied to neurons. Dorsomorphin was dissolved in DMSO to make a 1 mM stock solution. Neurons were incubated with Tyrodes containing Dorsomorphin for 25-30 min and the solution was replaced every 10 min without continuous perfusion.

GLUT4-pH Measurements

Vesicle pH in GLUT4-pH-containing vesicles was calculated as previously described (Sankaranarayanan et al., 2000) and surface fraction of GLUT4-pH before and after electrical stimulation was determined using the calculated pH value of 6.06. Maximal $\Delta F/\Delta F_{NH4Cl}$ of GLUT4-pH after stimulation was calculated by averaging 10 data points leading up to the peak. Since overexpression of DN AMPKα1 lowered ΔF_{NH4Cl} of GLUT4-pH, to calculate maximal $\Delta F/\Delta F_{NH4Cl}$ in Figure 4C, maximal $\Delta F/F_{initial}$ for each cell, control or overexpressing, was divided by the average $\Delta F_{NH4Cl}/ F_{initial}$ obtained from many control cells (which normalizes for expression level differences of control and DN AMPKα1).

Brain Slice Immunohistochemistry

Adult mouse brain was dissected after cardiac perfusion, post-fixed in 4% PFA/PBS overnight at 4°C, then cryopreserved in 10% sucrose/PBS for 2 days at 4°C. 20μm frozen sections were cut on a cryostat, coronally for hippocampal regions and sagittally for

cerebellar regions. Sections were permeablized with 0.05% Triton X-100/PBS, neutralized with 0.3M Glycine/0.05% Triton X-100/PBS, blocked and stained in 3% donkey serum/0.05% Triton X-100/PBS. The following primary antibodies were used: rabbit anti-GLUT4 antibody (Alomone Labs AGT-024, RRID: AB_2631197), guinea pig anti-VGLUT1 (Millipore AB5905, RRID: AB_2301751), mouse anti-Calbindin (SWANT C9638, RRID: AB_2314070). The secondary antibodies were: donkey anti-rabbit Alexa568, donkey-anti-guinea pig Alexa488, donkey-anti-mouse Alexa488, and Hoechst for nuclear counterstaining.

Dissociated Neuron Immunocytochemistry

Neurons were fixed with 4% paraformaldehyde, permeabilized with 0.2% Triton X-100, blocked with 5% BSA, and incubated with rabbit anti-GLUT4 antibody (see above) and guinea pig anti-synapsin 1/2 (Synaptic Systems 106-004, RRID: AB_1106784), or chicken anti-GFP (ThermoFisher Scientific A10263, RRID: AB_2534024) antibodies, followed by incubation with Alexa 546 or Alexa 568 and Alexa 488 secondary antibodies. Images were collected on Zeiss LSM 510 and LSM 880 confocal microscopes.

Validation of *Glut4* Knockdown by Immunostaining

Following transfection with VGLUT1-pH and *Glut4* shRNA or GLUT4-pH, neurons were fixed and stained with anti-GLUT4 antibody and anti-GFP antibody which also recognizes pHluorin. GLUT4 expression level was determined by selecting ROIs corresponding to the soma of neurons expressing VGLUT1-pH or GLUT4-pH and measuring the fluorescence intensity of GLUT4 immunofluorescence at the ROIs, followed by background subtraction (F_{trans}). The expression level of GLUT4 in boutons expressing GLUT4-pH was determined by selecting ROIs positive for synapsin I staining. GLUT4 immunofluorescence was similarly measured in neighboring untransfected neurons ($F_{untrans}$) in the same illumination field, and the change in expression level was calculated as $F_{trans}/F_{untrans}$ *100% for both *Glut4* KD and GLUT4 OE.

QUANTIFICATION AND STATISTICAL ANALYSIS

Image Analysis and Statistics

Images were analyzed using the ImageJ plugin Time Series Analyzer V3 where 10-20 regions of interest (ROIs) of ~2 μm corresponding to responding synaptic boutons were selected and the fluorescence was measured over time. All fitting was done with OriginPro v8 as previously described (Balaji and Ryan, 2007). Statistical analysis was performed with OriginPro v8 and GraphPad Prism v6.0 for PC. In most experiments, the Mann–Whitney U test was used to determine the significance of the difference between two conditions. For paired comparison of responses before and after treatment with dorsomorphin, the Kolmogorov-Smirnov test was used. $p < 0.05$ was considered significant and denoted with a single asterisk, whereas $p < 0.01$, $p < 0.001$ and $p < 0.0001$ are denoted with two, three, and four asterisks, respectively. The n value, indicated in the figure legends for each experiment, represents the number of cells imaged.

Quantification of Synaptic Vesicle Endocytic Block

The block in endocytosis of VGLUT1-pH in *Glut4* KD neurons or neurons treated with dGlu was quantified with varying stimulation intensities. For dGlu treatments, the fraction of VGLUT1-pH signal remaining at two endocytic constants (2τ) at the end of electrical stimulation, denoted as $\Delta F_{2\tau}/\Delta F_{max}$, was determined for each neuron before and after treatment using the τ of before treatment at each stimulation intensity. Endocytic block was calculated as $(\Delta F_{2\tau}/\Delta F_{max})_{after}/(\Delta F_{2\tau}/\Delta F_{max})_{before}$. In the case of *Glut4* KD neurons, $\Delta F_{2\tau}/\Delta F_{max}$ was calculated using average τ of control neurons for each stimulation intensity. Endocytic block for each *Glut4* KD neuron was measured as:

$$x = \frac{(\Delta F_{2\tau}/\Delta F_{max})_{Glut4KD}}{\text{mean}(\Delta F_{2\tau}/\Delta F_{max})_{control}}$$

The standard error for endocytic block of *Glut4* KD was determined as follows:

$$s.e.m = \frac{\sqrt{\sum_{i=1}^{n} S_{x_i}^2}}{\sqrt{n}},$$

$$S_{x_i} = x.S_{control}$$

Where S_{x_i}, the standard deviation for each value of endocytic block, and $S_{control}$ is the standard deviation of $(\Delta F_{2\tau}/\Delta F_{max})_{control}$ values.

Neuron, Volume *93*

Supplemental Information

GLUT4 Mobilization Supports Energetic Demands of Active Synapses

Ghazaleh Ashrafi, Zhuhao Wu, Ryan J. Farrell, and Timothy A. Ryan

Supplementary Figures

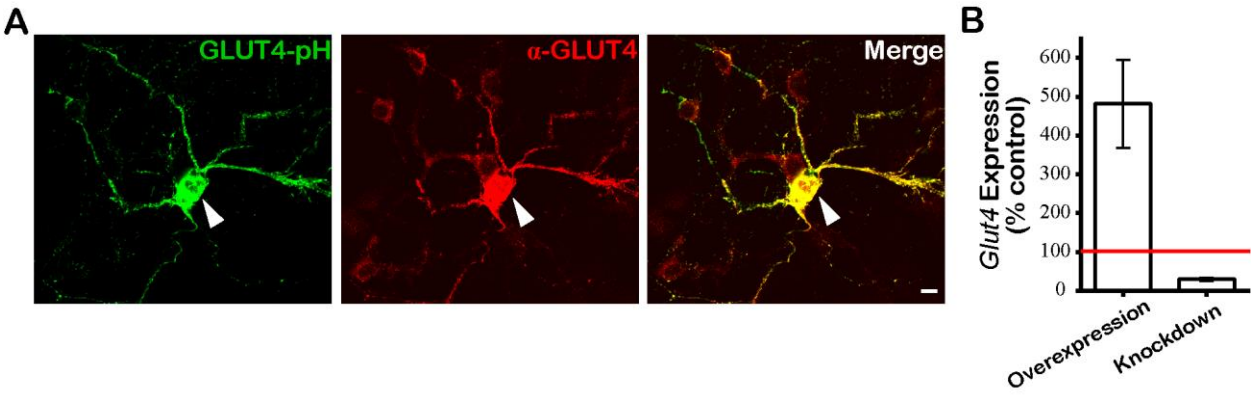

Figure S1 (related to Figure 1). Validation of GLUT4 antibody with overexpression and knockdown of *Glut4*. (A) Immunostaining of hippocampal neurons overexpressing GLUT4-pH (arrowhead) in a field of untransfected neurons stained with antibodies against endogenous GLUT4 (red) and pHluorin (green). GLUT4 immunofluorescence is increased in the transfected neuron, suggesting recognition of GLUT4 by the antibody. Scale bar, 10 µm. (B) GLUT4 level in the soma of neurons expressing VGLUT1-pH and *Glut4* shRNA or overexpressing GLUT4-pH normalized to untransfected neurons in the same field of view. Red horizontal line denotes 100% of control *Glut4* expression. Overexpression: 482 ± 113 %, knockdown: 30 ± 5 %; n = 5-24. Error bars are SEM.

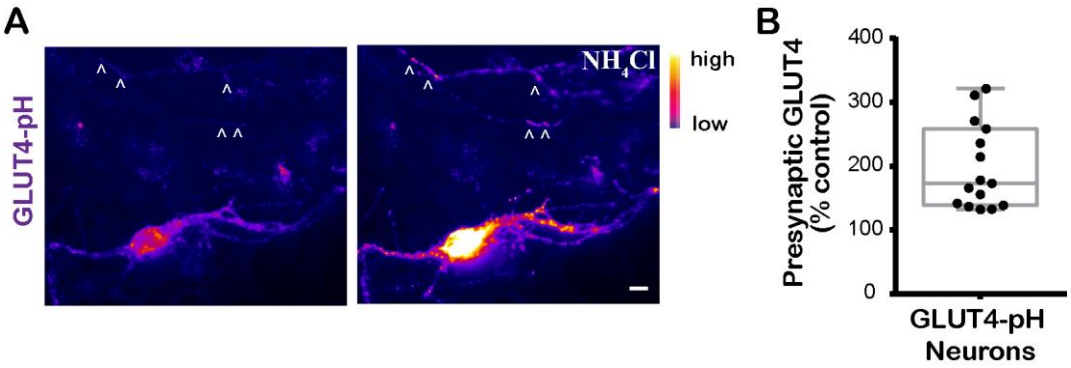

Figure S2 (related to Figure 2). GLUT4-pH expression in hippocampal neurons. (A) Pseudocolor images of GLUT4-pH at baseline or during treatment with NH_4Cl to

neutralize vesicle pH. Arrowheads point to axonal GLUT4-pH vesicles that are acidic and can be visualized with NH_4Cl. Scale bar, 10 µm. (B) Presynaptic GLUT4 levels colocalizing with synapsin in GLUT4-pH expressing neurons compared to control. The box and whisker plot represents median (line), 25th-75th percentile (box), and min-max (whisker). Mean (% control): 200 ± 20; n = 15 cells.

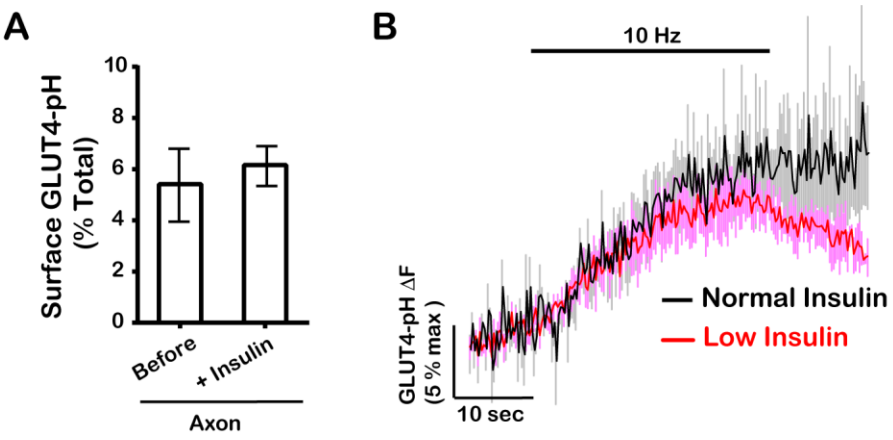

Figure S3 (related to Figure 2). Axonal GLUT4 is not sensitive to insulin. (A) Surface GLUT4-pH (% total) in axons does not change within 10 minutes of treatment with 8 µM insulin. Before: 5 ± 1, insulin: 6.2 ± 0.8; n = 6 cells. (B) Insulin deprivation for 24-48 hours does not affect GLUT4 mobilization in response to electrical stimulation (600 AP, 10 Hz). Error bars are shown as grey and pink lines. All error bars are SEM.

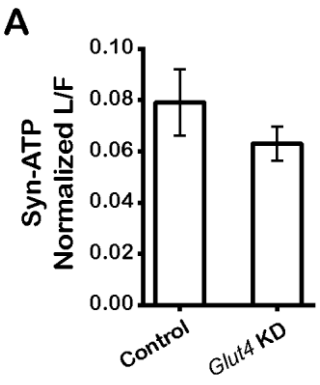

Figure S4 (related to Figure 4). Basal ATP level is not changed in *Glut4* KD neurons. (A) Syn-ATP luminescence to fluorescence ratio in *Glut4* KD and control boutons, pH corrected with cytoplasmic pHluorin. Control: 0.08 ± 0.01, *Glut4* KD: 0.063 ± 0.006; n = 5-6 cells. Error bars are SEM.

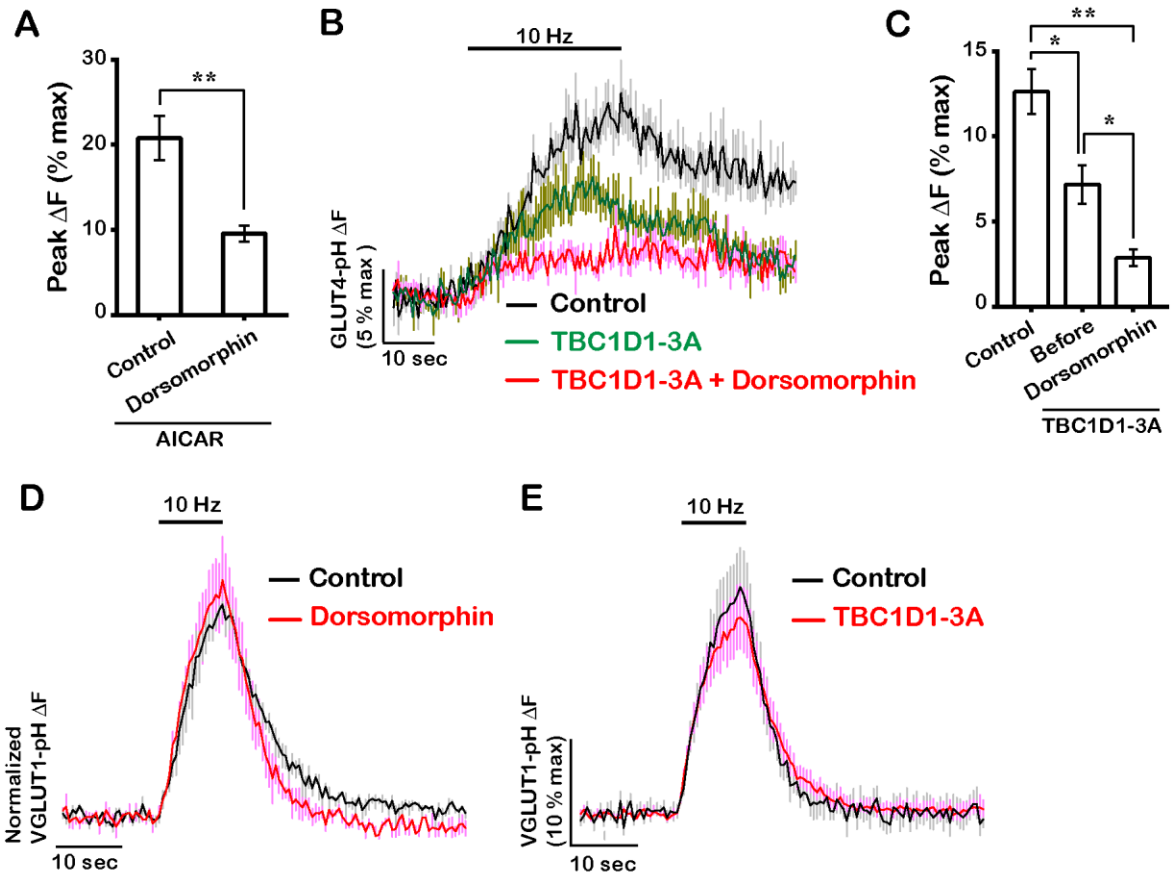

Figure S5 (related to Figure 7). Dorsomorphin and TBC1D1-3A impair GLUT4 mobilization but do not affect synaptic vesicle exocytosis. (A) Average maximal ΔF (% max) of GLUT4-pH in response to AICAR (1mM) in control neurons or neurons treated with 10 μM dorsomorphin for 30 minutes. Control: 20 ± 3, dorsomorphin: 10 ± 1; n = 6-13 cells. (B) Average traces of GLUT4-pH in response to stimulation with 300 AP (10Hz) in control neurons or neurons expressing TBC1D1-3A with or without dorsomorphin treatment. (C) Average maximal ΔF (% max) of GLUT4-pH shown in B.

Control: 13 ± 1, TBC1D1-3A-before: 7 ± 1, TBC1D1-3A-dorsomorphin: 2.9 ± 0.5; n = 6 cells per condition. (D, E) Average VGLUT1-pH traces of neurons (D) treated with dorsomorphin, (E) or expressing TBC1D1-3A are similar to control neurons. Error bars in graphs are shown in gray, pink and green (B, D, and E). All error bars are SEM.

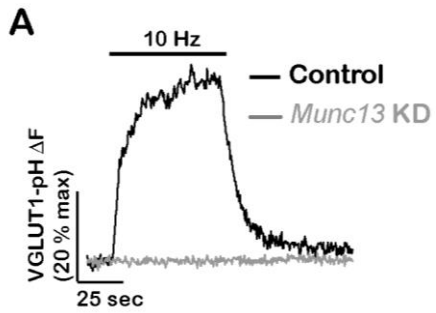

Figure S6 (related to Figure 8). MUNC13 is required for synaptic vesicle release.

(A) Sample VGLUT1-pH trace in response to electrical stimulation (600 AP, 10 Hz) in control and *Munc13* KD neurons.